Article

Cell Reports

HOIP Deficiency Causes Embryonic Lethality by Aberrant TNFR1-Mediated Endothelial Cell Death

Graphical Abstract

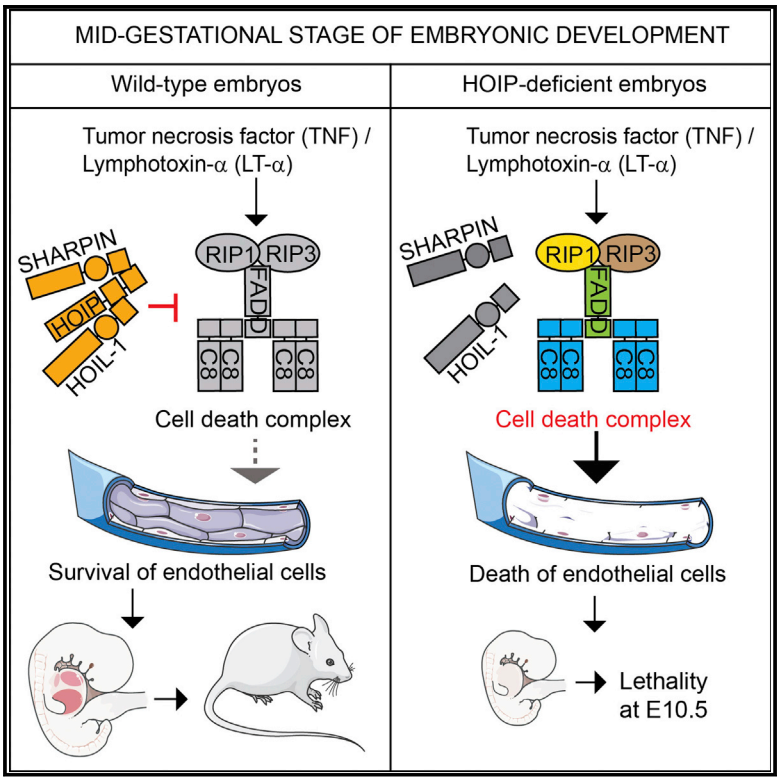

Highlights

Genetic ablation of HOIP results in embryonic lethality at midgestation (E10.5)

Conditional HOIP deletion in the endothelium is sufficient to cause embryonic death

Defective yolk sac vascularization is causative for embryonic lethality at E10.5

Aberrant TNFR1-mediated cell death is the cause of defective vascularization

Authors

Nieves Peltzer, Eva Rieser, ..., Tristan A. Rodriguez, Henning Walczak

Correspondence

h.walczak@ucl.ac.uk

In Brief

HOIP is the main catalytic subunit of the linear ubiquitin chain assembly complex (LUBAC), a crucial regulator of TNF and other immune signaling pathways. Peltzer et al. find that HOIP deficiency results in embryonic lethality at midgestation due to endothelial cell death mediated by TNFR1. Aberrant formation of a TNF-mediated cell-death-inducing complex in HOIP-deficient (but not -proficient) cells underlies the phenotype, with the catalytic activity of HOIP required for the control of cell death in response to TNF.

Peltzer et al., 2014, Cell Reports 9, 153–165
October 9, 2014
http://dx.doi.org/10.1016/j.celrep.2014.08.066

CellPress

Cell Reports
Article

HOIP Deficiency Causes Embryonic Lethality by Aberrant TNFR1-Mediated Endothelial Cell Death

Nieves Peltzer,[1,6] Eva Rieser,[1,6] Lucia Taraborrelli,[1] Peter Draber,[1] Maurice Darding,[1] Barbara Pernaute,[2] Yutaka Shimizu,[1] Aida Sarr,[1] Helena Draberova,[1] Antonella Montinaro,[1] Juan Pedro Martinez-Barbera,[3] John Silke,[4,5] Tristan A. Rodriguez,[2] and Henning Walczak[1,*]

[1]Centre for Cell Death, Cancer, and Inflammation (CCCI), UCL Cancer Institute, University College London, 72 Huntley Street, London WC1E 6DD, UK
[2]British Heart Foundation Centre for Research Excellence, National Heart and Lung Institute (NHLI), Imperial Centre for Translational and Experimental Medicine, Imperial College London, Hammersmith Hospital Campus, Du Cane Road, London W12 0NN, UK
[3]Birth Defects Research Centre, Developmental Biology and Cancer Programme, UCL Institute of Child Health, London WC1N 1EH, UK
[4]The Walter and Eliza Hall Institute of Medical Research, Parkville, VIC 3052, Australia
[5]Department of Medical Biology, University of Melbourne, Parkville, VIC 3050, Australia
[6]Co-first author
*Correspondence: h.walczak@ucl.ac.uk
http://dx.doi.org/10.1016/j.celrep.2014.08.066

SUMMARY

Linear ubiquitination is crucial for innate and adaptive immunity. The linear ubiquitin chain assembly complex (LUBAC), consisting of HOIL-1, HOIP, and SHARPIN, is the only known ubiquitin ligase that generates linear ubiquitin linkages. HOIP is the catalytically active LUBAC component. Here, we show that both constitutive and Tie2-Cre-driven HOIP deletion lead to aberrant endothelial cell death, resulting in defective vascularization and embryonic lethality at midgestation. Ablation of tumor necrosis factor receptor 1 (TNFR1) prevents cell death, vascularization defects, and death at midgestation. HOIP-deficient cells are more sensitive to death induction by both tumor necrosis factor (TNF) and lymphotoxin-α (LT-α), and aberrant complex-II formation is responsible for sensitization to TNFR1-mediated cell death in the absence of HOIP. Finally, we show that HOIP's catalytic activity is necessary for preventing TNF-induced cell death. Hence, LUBAC and its linear-ubiquitin-forming activity are required for maintaining vascular integrity during embryogenesis by preventing TNFR1-mediated endothelial cell death.

INTRODUCTION

Ubiquitination is the covalent attachment of ubiquitin to a target protein. When ubiquitin itself is the target, interubiquitin linkages are formed. Eight amino groups within the ubiquitin moiety, namely the respective ε-amino groups on its seven lysines and the α-amino group on the amino-terminal methionine (M1), can serve as acceptor for the terminal carboxyl group of the incoming ubiquitin. Thereby, eight structurally and functionally distinct diubiquitin linkage types can be generated (Komander, 2009). The ubiquitin linkage resulting from the use of M1 of ubiquitin, the so-called linear ubiquitin linkage, is involved in gene activation and regulates inflammation and cell death in several innate and adaptive immune signaling pathways (Iwai et al., 2014; Rieser et al., 2013; Walczak et al., 2012). The linear ubiquitin chain assembly complex (LUBAC) is currently the only known E3 ligase that generates linear linkages under physiological conditions and is composed of three proteins—heme-oxidized iron-responsive element-binding protein 2 (IRP2) ubiquitin ligase-1 (HOIL-1; also known as RanBP-type and C3HC4-type zinc finger-containing protein 1 [RBCK1]), HOIL-1 interacting protein (HOIP; also known as ring finger protein 31 [RNF31]), and SH3 and multiple ankyrin repeat domains protein (SHANK)-associated RBCK1 homology (RH)-domain-interacting protein (SHARPIN; also known as SHANK-interacting protein-like 1 [SIPL1]) (Gerlach et al., 2011; Ikeda et al., 2011; Tokunaga et al., 2011)—with HOIP being the catalytically active component of this complex (Tokunaga et al., 2009).

LUBAC has been identified to regulate various signaling pathways that promote canonical NF-κB activation, including the ones triggered by tumor necrosis factor (TNF), nucleotide oligomerization domain 2 (NOD2), interleukin 1 (IL-1), and Toll-like receptor 2 (TLR2) and TLR4 (Damgaard et al., 2012; Emmerich et al., 2013; Gerlach et al., 2011; Sasaki et al., 2013; Zak et al., 2011; Zinngrebe et al., 2014). The best-characterized pathway involving LUBAC is the one triggered by tumor necrosis factor receptor 1 (TNFR1) activation. The crucial hub in this pathway is the TNFR1-signaling complex (TNF-RSC). Upon binding to TNF, TNFR1 oligomerizes, resulting in recruitment of TRADD, TRAF2, cIAP1/2, and RIP1. cIAP1/2-mediated ubiquitination of components of the TNF-RSC leads to recruitment of the TAK1-TAB1-TAB2 complex for mitogen-activated protein kinase (MAPK) activation and of LUBAC. LUBAC in turn forms linear ubiquitin linkages on RIP1 and NEMO/IKKγ, stabilizing and activating the IKKα-IKKβ-NEMO/IKKγ complex for optimal NF-κB activation (Gerlach et al., 2011; Schmukle and Walczak, 2012). Alternatively, when the TNF-RSC is destabilized by inhibition, absence, or malfunction of its components, a secondary cytoplasmic complex, known as complex-II, is formed around RIP1

A

Stage	*Hoip*$^{+/+}$	*Hoip*$^{+/-}$	*Hoip*$^{-/-}$	Total
Weaned mice	42 (32)	86 (64)	0 (32)	128
Emb at E11.5	8 (8)	18 (16)	1+5* (8)	32
Emb at E10.5	18 (16.75)	36 (33.5)	13 (16.75)	67
Emb at E9.5	9 (9.5)	18 (18.5)	10 (9.25)	37

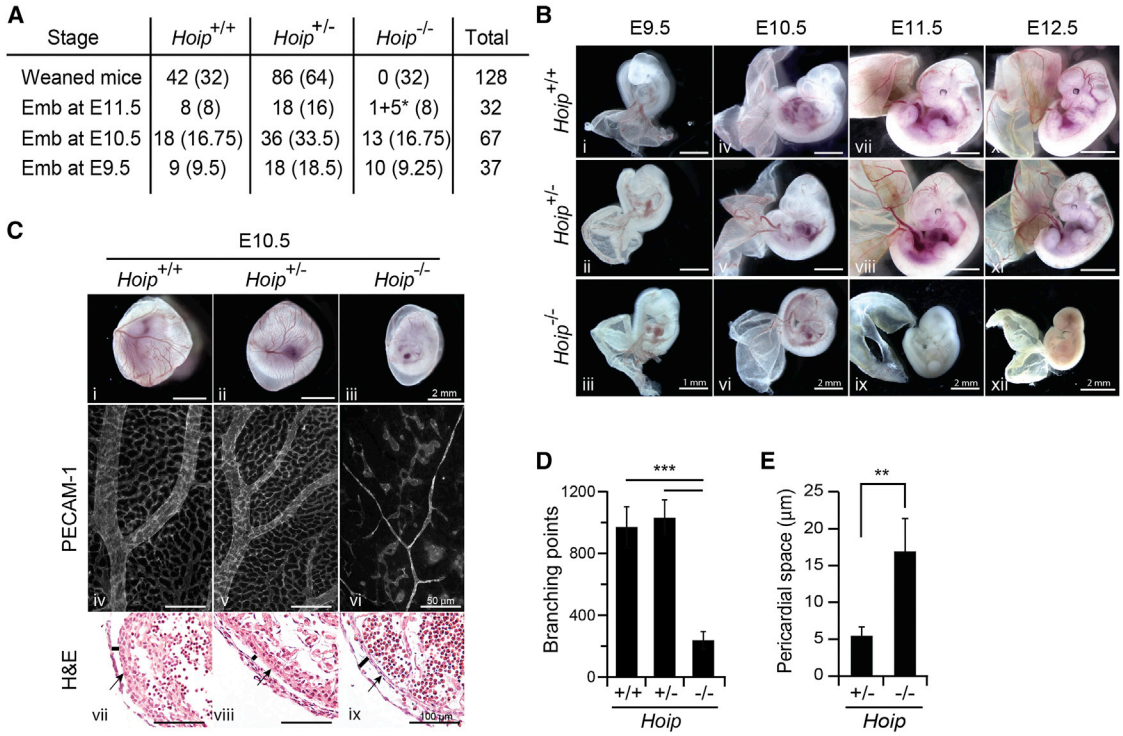

Figure 1. HOIP Deficiency Results in Embryonic Lethality at Midgestation

(A) Quantification of genotypes of animals obtained after intercrossing *Hoip*$^{+/-}$ mice. Expected values according to Mendelian frequencies are indicated in brackets. *Dead.

(B) Time-line of the embryonic development of *Hoip*$^{+/+}$, *Hoip*$^{+/-}$, and *Hoip*$^{-/-}$ embryos from E9.5 to E12.5. E9.5 *Hoip*$^{-/-}$ embryos appeared normal (i–iii), whereas E10.5 embryos lacked vascularization in the yolk sac and were smaller compared to wild-type littermates (iv–vi). At E11.5 and E12.5, embryos were dead (vii–ix and x–xii, respectively). Heterozygosity of *Hoip* has no detectable aberration. See also Figure S1D.

(C) Vascular defects at E10.5 are shown macroscopically (i–iii) and microscopically by PECAM-1 staining in yolk sacs (iv–vi). Histological analysis revealed heart defects such as enlargement of the pericardial cavity (black line) and thinning of the ventricular wall (arrow) (vii–ix). See also Figure S1E.

(D) Branching point quantification of images in (C) (iv–vi). Statistics were performed by ANOVA for multiple comparisons. Data are presented as mean ± SEM (n = 3 yolk sacs).

(E) Quantification of the pericardial space was performed on five serial sections of the heart for each embryo. Data are presented as mean ± SEM (n = 3 embryos).

involving caspase-8, FADD, cFLIP, and RIP3. This complex induces cell death by apoptosis or necroptosis (Micheau and Tschopp, 2003; Tenev et al., 2011).

The essential role of LUBAC in TNF signaling was evidenced in mice lacking SHARPIN (chronic proliferative dermatitis mice [*cpdm*]), which develop a spontaneous inflammatory syndrome (Seymour et al., 2007). We and others previously showed that cells derived from *cpdm* mice have decreased NF-κB activation and are more sensitive to TNF-induced cell death (Gerlach et al., 2011; Ikeda et al., 2011; Tokunaga et al., 2011). Importantly, we could further show that deletion of TNF in *cpdm* mice completely rescued them from the inflammatory disease (Gerlach et al., 2011). Together, these results suggested TNF-dependent cell death as causative for the inflammatory manifestations of the *cpdm* phenotype. However, as linear ubiquitination is only suppressed, but not abolished, in the absence of SHARPIN, the effect of a complete lack in LUBAC activity on physiology is unknown. We therefore examined the physiological role of the catalytically active LUBAC component, HOIP, by studying mice deficient for this component. Here, we report that HOIP deletion leads to embryonic lethality at midgestation due to TNFR1-mediated aberrant death of endothelial cells, disrupting the vascular architecture.

RESULTS

HOIP Deficiency Results in Embryonic Lethality

HOIP-deficient C57BL/6 mice were obtained as described in Experimental Procedures (Figures S1A and S1B). Among more than 100 progeny from *Hoip* heterozygous mouse intercrosses, not a single mouse with homozygous deletion in the *Hoip* gene was born, indicating that HOIP deficiency results in embryonic lethality (Figure 1A). Western blotting of whole embryos confirmed HOIP absence and revealed a substantial concomitant decrease in HOIL-1 and SHARPIN expression (Figure S1C), in line with previous observations in vitro (Gerlach et al., 2011; Tokunaga et al., 2011).

To define the embryonic stage at which HOIP-deficient (*Hoip*$^{-/-}$) embryos die, embryos were analyzed at different days of gestation. No morphological differences among *Hoip*$^{+/+}$, *Hoip*$^{+/-}$, and *Hoip*$^{-/-}$ embryos were detected at 8 and 9 days of embryonic development (E8.5–E9.5) (Figure S1D;

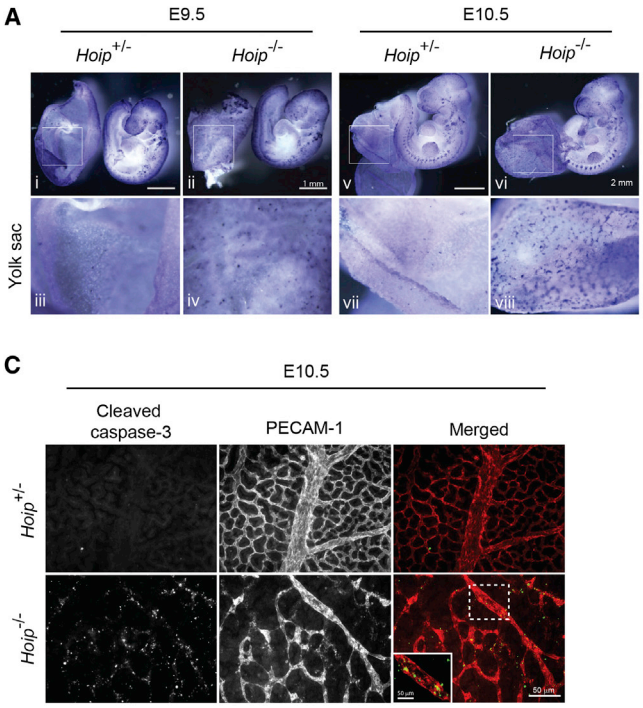

Figure 2. HOIP Deficiency Leads to Exacerbated Cell Death Induction

(A) Representative images of cell death as detected by whole-mount TUNEL staining. In *Hoip*$^{-/-}$ embryos, cell death was observed mainly in yolk sacs first appearing at E9.5 (i–iv) and significantly increasing at E10.5 (v–viii). Images (iii) and (iv) and (vii) and (viii) are magnifications of the indicated regions of the yolk sac. See also Figures S2A and S2E.

(B) Quantification of cell death observed in (A). Data are presented as mean ± SEM (n = 3 embryos). AU, arbitrary units.

(C) Cleaved caspase-3 and PECAM-1 double staining in yolk sacs. Merged images show co-localization of cleaved caspase-3 (green) and PECAM-1 (red). See also Figure S2F.

(D) Quantification of cleaved-caspase-3-positive cells. Data are presented as mean ± SEM (n = 3 yolk sacs). See also Figure S2B.

Figures 1B i–iii). At E10.5, however, *Hoip*$^{-/-}$ embryos were small and had aberrant vascularization with only few major vessels detected macroscopically (Figures 1B iv–vi and 1C i–iii). These embryos were resorbed at E11.5/12.5 (Figures 1B vii–ix and x–xii, respectively). Thus, *Hoip*$^{-/-}$ embryos die at E10.5.

Since absence of proper yolk sac vascularization could cause embryonic lethality, we examined the yolk sac endothelium in more detail. Staining of PECAM-1, an endothelial cell marker, revealed severe vascular architectural defects with decreased vascular density as determined by quantification of vessel branching points (Figures 1C iv–vi and 1D). Histological analysis showed abnormalities mainly in the embryos' hearts with enlargement of the pericardial space (Figures 1C vii–ix and 1E) and marked attenuation of the ventricular wall (Figures 1C vii–ix), features associated with decreased vascular density in the yolk sac and, hence, less blood arriving at the heart. At E9.5, yolk sac vascularization was already affected, albeit mildly, whereas no aberrant phenotype was observed in the heart (Figures S1E and S1F). Thus, although defects start to appear at E9.5, the phenotype is manifest at E10.5, and nearly all embryos are dead by E11.5.

Importantly, *Hoip* is ubiquitously expressed at E10.5 as determined by in situ hybridization in wild-type embryos (Figure S1G), indicating that the vascular phenotype is a consequence of HOIP being required for normal vascularization at this developmental stage, rather than resulting from specific expression of HOIP in the vasculature.

Hoip$^{-/-}$ Embryos Suffer from Excessive Endothelial Cell Death at Midgestation

To study the cause of the disrupted vasculature in yolk sacs of *Hoip*$^{-/-}$ embryos, we analyzed cell death by whole-mount TUNEL staining. At E8.5, no difference was observed between *Hoip*$^{-/-}$ and *Hoip*$^{+/-}$ embryos (Figure S2A). However, at E9.5, *Hoip*$^{-/-}$ embryos showed a significant increase in TUNEL-positive cells (Figures 2A i–iv and 2B), and by E10.5, this difference was dramatic, correlating with near-complete disruption of yolk sac vascular architecture (Figures 2A v–viii and 2B) and increased cell death in the heart of HOIP-deficient embryos (Figures S2C and S2D). At E11.5, massive cell death in the yolk sac and in the embryo proper, particularly in heart and forebrain, was observed, correlating with resorption (Figure S2E).

Using cleaved caspase-3 as a marker of apoptotic cells, we found that apoptosis was increased in *Hoip*$^{-/-}$ yolk sacs at E9.5 (Figure S2B) and that this increase was even more pronounced at E10.5 (Figures 2C and 2D). At E11.5, cleaved caspase-3 was also detected in vessels throughout the embryo (Figure S2F) correlating with disruption of vascular architecture and death. As cleaved caspase-3 was present in PECAM-1^{+} cells (Figure 2C), apoptosis occurred in endothelial cells. These results suggest that in *Hoip*$^{-/-}$ embryos, excessive apoptosis of endothelial cells, most likely starting at E9.5 in the yolk sac and spreading over the next few days of embryonic development throughout the embryo (note that vascularization in the embryo proper is affected at E11.5, but not at E10.5; Figure S2F), could be responsible for vascular defects and, consequently, lethality.

Endothelial Deletion of *Hoip* Phenocopies Constitutive *Hoip* Deletion

To evaluate whether HOIP deficiency in endothelial cells was indeed responsible for embryonic lethality at E10.5, we aimed to specifically delete HOIP from endothelial cells by crossing *Hoip*$^{fl/fl}$ mice with mice expressing the Cre recombinase under the control of the endothelium-specific Tie2 promoter (*Hoip*$^{fl/fl}$ *Tie2-Cre*+). We identified only three *Hoip*$^{fl/fl}$*Tie2-Cre*+ at weaning compared to an expected 36.5 mice (Figure S3A; Figure 3A), suggesting that HOIP deficiency in endothelial cells is sufficient to cause embryonic lethality. It is likely that the three mice that

A

Stage	$Hoip^{fl/wt}$ Tie2-Cre-	$Hoip^{fl/wt}$ Tie2-Cre+	$Hoip^{fl/fl}$ Tie2-Cre-	$Hoip^{fl/fl}$ Tie2-Cre+	Total
Weaned mice	56 (36.5)	48 (36.5)	39 (36.5)	3 (36.5)	146
Emb at E11.5	1 (4)	4 (4)	6 (4)	5*(4)	16
Emb at E10.5	9 (8.75)	10 (8.75)	8 (8.75)	8 (8.75)	35
Emb at E9.5	4 (5)	3 (5)	9 (5)	4 (5)	20

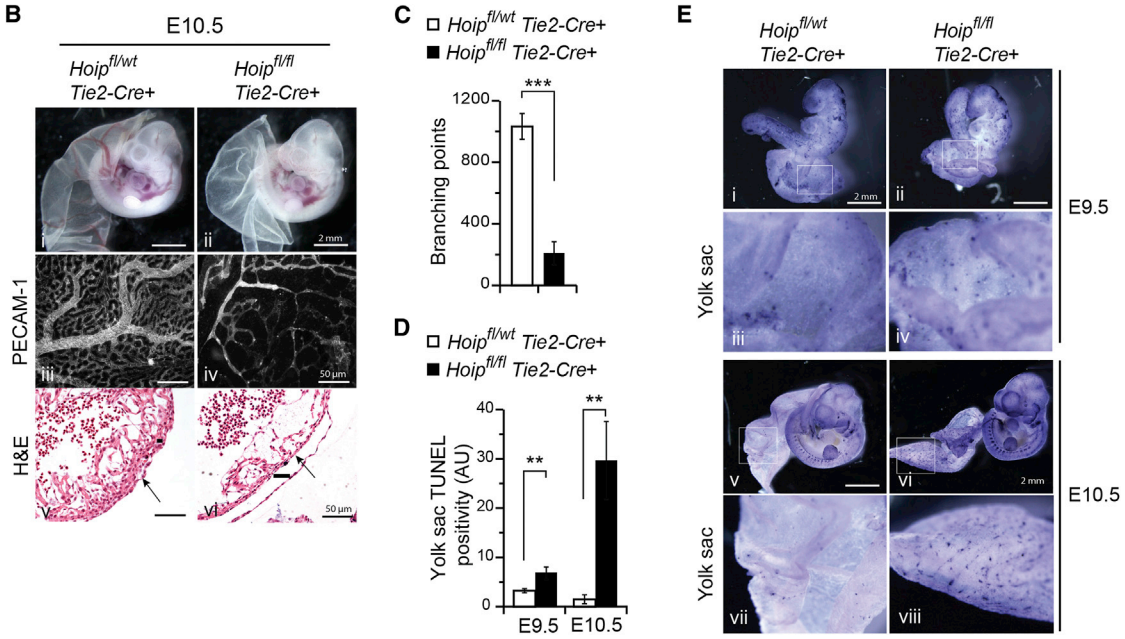

Figure 3. HOIP Deficiency in Endothelium Results in Embryonic Lethality at E10.5

(A) Quantification of genotypes of animals obtained after crossing $Hoip^{fl/wt}$*Tie2-Cre*+ males with $Hoip^{fl/fl}$*Tie2-Cre*- females. Expected values according to Mendelian frequencies are indicated in brackets. *Dead or resorbed embryos.

(B) $Hoip^{fl/fl}$*Tie2-Cre*+ embryos died at E10.5 with vascular defects as shown macroscopically (i and ii) and microscopically by PECAM-1 staining (iii and iv). Histology revealed defects in the heart such as enlargement of the pericardial cavity (black line) and thinning of the ventricular wall (arrow) (v and vi). See also Figure S3B.

(C) Branching point quantification of images in (B) (iii and iv). Data are presented as mean ± SEM (n = 3 yolk sacs).

(D) Quantification of cell death shown in (E). Data are presented as mean ± SEM (n = 3 yolk sacs). AU, arbitrary units.

(E) Cell death analysis by whole-mount TUNEL staining showing gradual increase in cell death from E9.5 (i–iv) to E10.5 (v–viii). Images (iii) and (iv) and (vii) and (viii) are magnifications of the indicated regions of the yolk sac.

survived embryonic development had incomplete penetrance of the Tie2-Cre-mediated deletion.

Like embryos with germline deletion of *Hoip*, $Hoip^{fl/fl}$*Tie2-Cre*+ embryos appeared normal at early developmental stages up to E9.5 (Figure S3B i and ii) but died at E10.5 with disrupted vascularization, as observed macroscopically (Figures 3B i and ii) and microscopically by PECAM-1 staining (Figures 3B iii and iv and 3C), and were resorbed at E11.5 (Figure S3B iii and iv). As a consequence of decreased vascular density, $Hoip^{fl/fl}$*Tie2-Cre*+ embryos also showed signs of cardiovascular failure with enlargement of the pericardial space and thinning of the ventricular wall (Figures 3B v and vi). Cell death analysis revealed presence of dying cells in yolk sacs of $Hoip^{fl/fl}$*Tie2-Cre*+ embryos, precisely as in $Hoip^{-/-}$ embryos, with TUNEL-positive cells first appearing at E9.5 (Figures 3D and 3E i–iv) and increasing substantially by E10.5 (Figures 3D and 3E v–viii). As with $Hoip^{-/-}$ embryos, dead cells were also present in hearts of $Hoip^{fl/fl}$*Tie2-Cre*+ embryos at E10.5 (Figure S3C).

As the Tie2 promoter is known to be activated early during embryogenesis (i.e., at E7.5) and thus before separation of the endothelial from the immune cell lineage (Haar and Ackerman, 1971; Hamaguchi et al., 2006), we checked whether HOIP deletion also occurred in immune cells of $Hoip^{fl/fl}$*Tie2-Cre*+ embryos. This was indeed the case, as confirmed by genotyping $CD31^+$ ($PECAM\text{-}1^+$) and $CD45^+$ cells sorted from Cre+ and Cre− embryos (Figure S3D). In order to assess viability of immune cells in $Hoip^{fl/fl}$*Tie2-Cre*+ embryos, we analyzed the percentage of living $CD45^+$ cells by flow cytometry at E9.5 and E10.5 in whole embryos, including yolk sacs. At E9.5, we observed no effect of HOIP deficiency on immune cell viability (Figure S3E), while death of endothelial cells in the yolk sacs of these embryos was readily observed at this time (Figure 3D). At E10.5, however, there is a reduction in the percentage of the immune cell population. Therefore, although endothelial cell death appears to be the first, and hence probably triggering, event in yolk sacs of $Hoip^{-/-}$ embryos, immune cells are also affected.

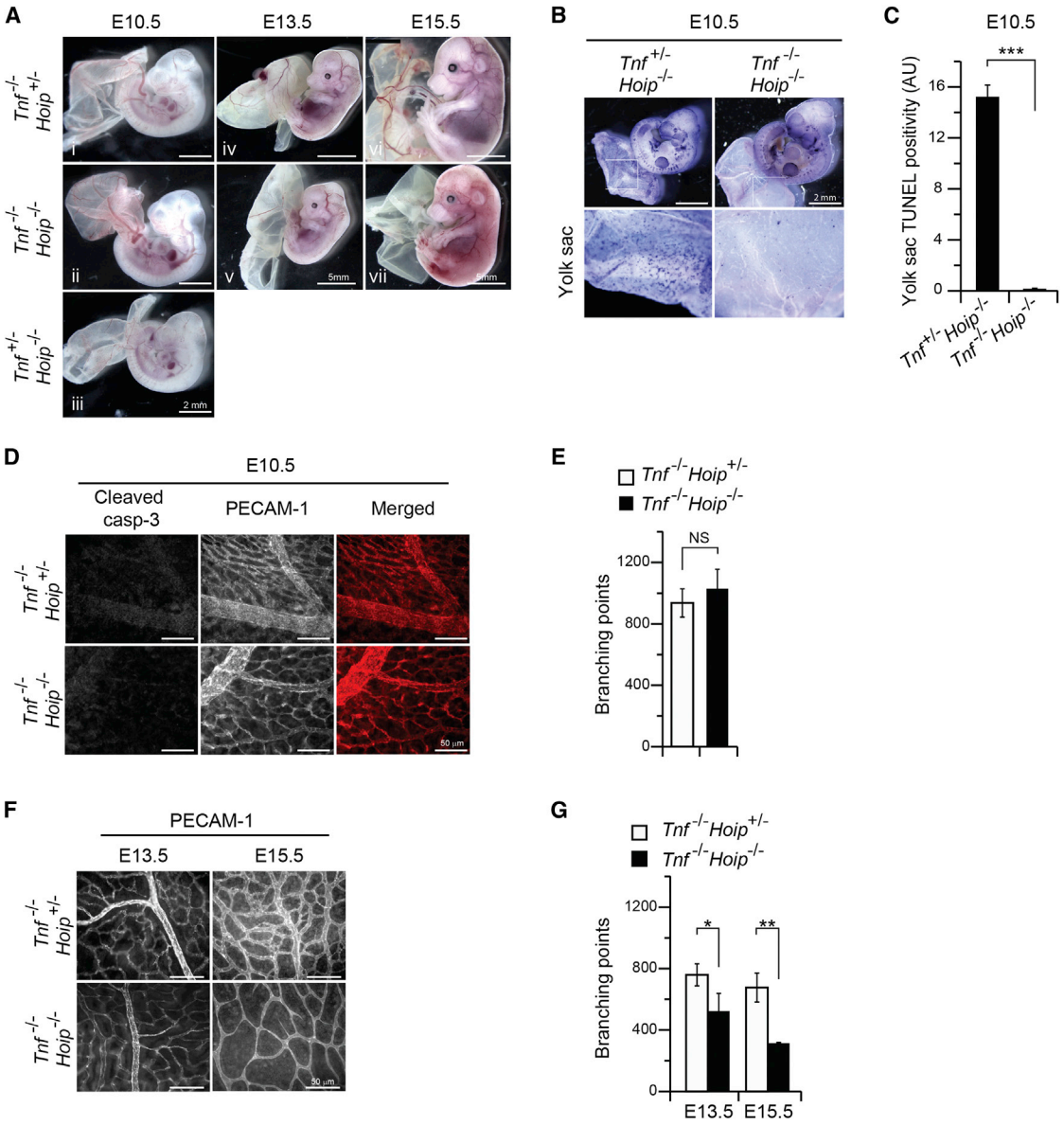

Figure 4. Ablation of TNF Prolongs Survival by Preventing Endothelial Cell Death at Midgestation, but Not Late Gestation

(A) Representative images of $Tnf^{-/-}Hoip^{+/-}$, $Tnf^{-/-}Hoip^{-/-}$, and $Tnf^{+/-}Hoip^{-/-}$ embryos at different developmental stages. At E10.5, deletion of TNF recues the lethality (i–iii). At E13.5, $Tnf^{-/-}Hoip^{-/-}$ embryos are alive but yolk sacs seemed poorly vascularized (iv and v). At E15.5, $Tnf^{-/-}Hoip^{-/-}$ embryos appear dead with absent vascularization in yolk sacs (vi and vii).

(B) Cell death analysis by whole-mount TUNEL staining at E10.5 showing complete prevention of cell death upon TNF deletion.

(C) Quantification of cell death analysis shown in (B). Data are presented as mean ± SEM (n = 3 yolk sacs) AU, arbitrary units.

(D) Representative images of cleaved caspase-3 (green) and PECAM-1 (red) double staining in yolk sacs at E10.5 showing no cell death and normal vascularization.

(E) Quantification of branching points as detected in the images in (D) (PECAM-1). Data are presented as mean ± SEM (n = 3 yolk sacs).

(F) Representative images of PECAM-1 staining of yolk sacs at different developmental stages (E13.5 and 15.5).

(G) Quantification of branching points as detected in the images in (F). Data are presented as mean ± SEM (n = 3 yolk sacs).

TNF Deletion Prevents Cell Death at Midgestation and Prolongs Survival of *Hoip*$^{-/-}$ Embryos

Given that LUBAC is essential for regulating TNF-induced cell death (Gerlach et al., 2011; Ikeda et al., 2011; Tokunaga et al., 2011) and that TNF ablation prevented inflammation in *cpdm* mice (Gerlach et al., 2011), we reasoned that TNF could also cause endothelial cell death in $Hoip^{-/-}$ embryos. If this were the case, absence of TNF from $Hoip^{-/-}$ embryos should overcome lethality at E10.5. Indeed, genetic codeletion of *Tnf* in $Hoip^{-/-}$ mice rescued normal embryonic development and vascularization at midgestation (Figures 4A i–iii, 4D, and 4E). Whole-mount TUNEL and cleaved caspase-3 staining in yolk

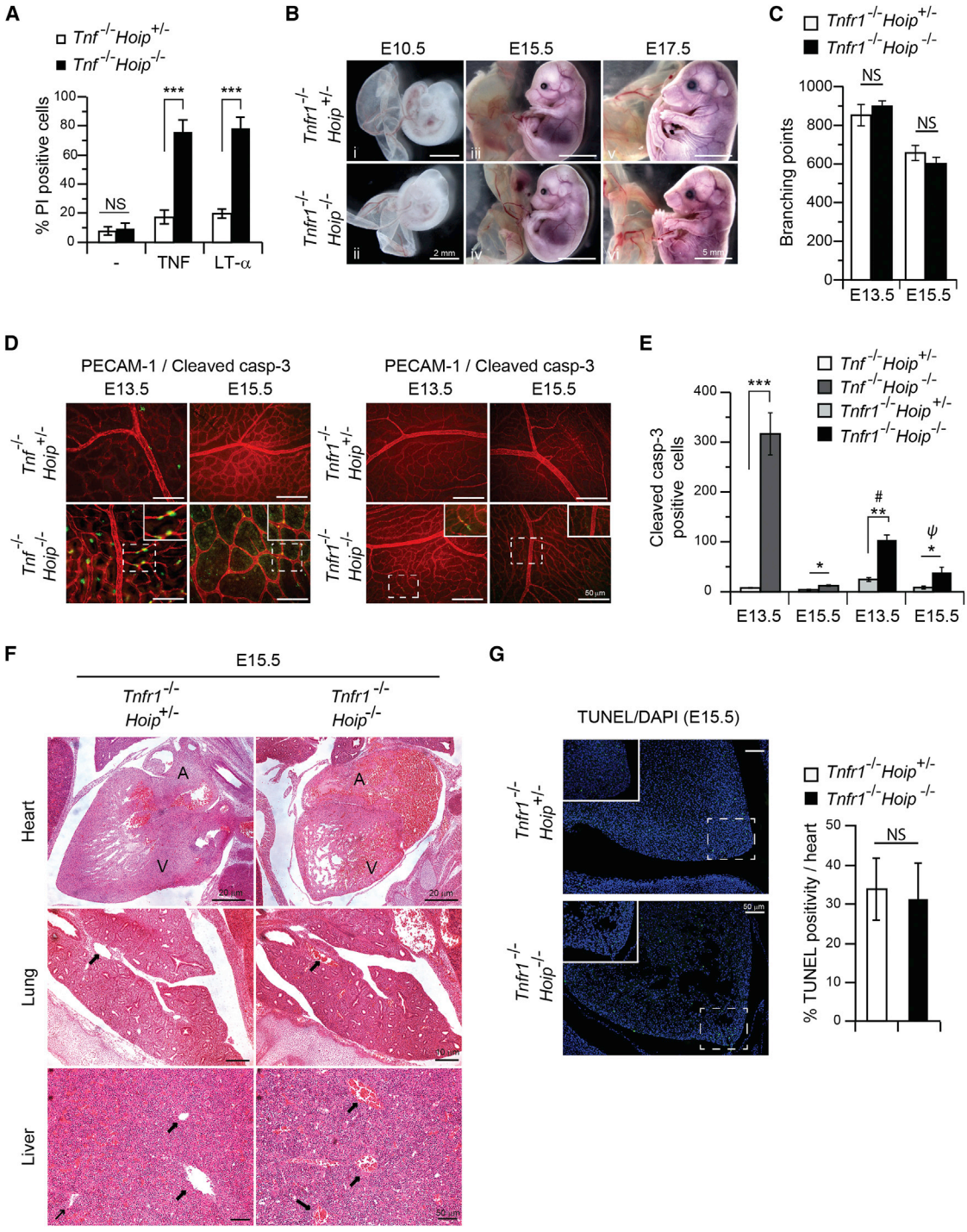

Figure 5. Ablation of TNFR1 Rescues Cell Death at Late Gestation and Completely Prevents Vascularization Defects

(A) Cell death analysis as measured by propidium iodide (PI) incorporation and flow cytometry in *Tnf*$^{-/-}$*Hoip*$^{-/-}$ MEFs stimulated with TNF (100 ng/ml) or LT-α (50 ng/ml) for 24 hr. Data are presented as mean ± SEM (n = 3 independent experiments).

(B) Representative images of *Tnfr1*$^{-/-}$*Hoip*$^{+/-}$ and *Tnfr1*$^{-/-}$*Hoip*$^{-/-}$ embryos at different developmental stages. At E10.5, deletion of TNFR1 rescues the lethality (i and ii). At E15.5, *Tnfr1*$^{-/-}$*Hoip*$^{-/-}$ embryos are alive and look properly vascularized (iii and iv). At E17.5, *Tnfr1*$^{-/-}$*Hoip*$^{-/-}$ embryos appear smaller, but the yolk sac vascularization appears normal (v and vi). See also Figure S5A.

(C) Quantification of branching points as determined by PECAM-1 staining. Data are presented as mean ± SEM (n = 3 yolk sacs). See also Figure S5C.

(D) Representative images of cleaved caspase-3 (green) and PECAM-1 (red) staining of yolk sacs at E13.5 and E15.5 in *Tnf*$^{-/-}$*Hoip*$^{-/-}$ versus *Tnfr1*$^{-/-}$*Hoip*$^{-/-}$. See also Figure S5D.

(legend continued on next page)

sacs of *Tnf*$^{-/-}$*Hoip*$^{+/-}$ versus *Tnf*$^{-/-}$*Hoip*$^{-/-}$ embryos at E10.5 showed a complete rescue from cell death in double mutants (Figures 4B–4D). We therefore conclude that loss of vascular architecture in *Hoip*$^{-/-}$ embryos at E10.5 is due to TNF-mediated endothelial cell death.

Despite rescuing *Hoip*$^{-/-}$ embryos from lethality at midgestation, genetic ablation of *Tnf* did not result in *Tnf*$^{-/-}$*Hoip*$^{-/-}$ mice being born (Figures S4A and S4B). Therefore, we studied *Tnf*$^{-/-}$*Hoip*$^{-/-}$ embryos at different stages of development to determine time and cause of death. Until E13.5, *Tnf*$^{-/-}$*Hoip*$^{-/-}$ embryos appeared normal, while their yolk sacs were already less vascularized than those of control embryos (Figures 4A iv and v). At E15.5, *Tnf*$^{-/-}$*Hoip*$^{-/-}$ embryos were dead and their yolk sacs completely deprived of macroscopically visible vessels (Figures 4A vi and vii). Analysis of the endothelial phenotype by PECAM-1 staining revealed that at E13.5, *Tnf*$^{-/-}$*Hoip*$^{-/-}$ embryos started losing vascular density (Figures 4F and 4G). This was further aggravated at E15.5 (Figure 4F and G), when yolk sacs were completely devoid of major vessels, both macro- and microscopically (Figures 4A vii and 4F). The fact that we could only detect vessels microscopically by PECAM-1 staining, and not macroscopically, is likely due to deprivation of blood supply as a consequence of endothelial cell death, which renders vessels undetectable macroscopically, whereas they remain detectable by staining for specific endothelial cell markers. Together, these results suggest that disruption of vascular architecture, even if delayed, is also causative for embryonic lethality at E15.5 in *Tnf*$^{-/-}$*Hoip*$^{-/-}$ embryos.

TNFR1, but Not TNF, Deletion Markedly Reduces Cell Death and Restores Normal Vascularization

Apart from TNF, lymphotoxin-α (LT-α) also engages with and signals through TNFR1 (Aggarwal et al., 1985). Indeed, we found that murine embryonic fibroblasts (MEFs) obtained from *Tnf*$^{-/-}$*Hoip*$^{-/-}$ embryos (we used *Tnf*$^{-/-}$*Hoip*$^{-/-}$ embryos to facilitate generation of MEFs deficient in HOIP) were rendered sensitive to death induction by both TNF and LT-α (Figure 5A), in line with the recently reported finding that SHARPIN-deficient cells are sensitized to TNF and LT-α (Etemadi et al., 2013). On this basis we hypothesized that TNF deletion might be insufficient to fully correct the vascular defects because of an additional effect of LT-α on TNFR1. We therefore generated *Tnfr1*$^{-/-}$*Hoip*$^{-/-}$ animals and, in accordance with our hypothesis, *Tnfr1*$^{-/-}$*Hoip*$^{-/-}$ embryos underwent early embryogenesis with normal vascularization and complete prevention of cell death in the yolk sac (Figures 5B i and ii; Figure S5B). Importantly, *Tnfr1*$^{-/-}$*Hoip*$^{-/-}$ embryos survived past E15.5 (Figures 5B iii and vi). Yet, at E17.5, the incidence of living embryos was not 100% (Figure S5A). Studying yolk sac vascularization at various developmental stages up to the time of death revealed that yolk sacs of *Tnfr1*$^{-/-}$*Hoip*$^{-/-}$ embryos appeared normally vascularized throughout development, including at E13.5 and E15.5 and in embryos still alive at E17.5 (Figure 5C; Figures S5C and S5D). Thus, TNF and LT-α together are responsible for the gradual loss of the vascular network up to late developmental stages in *Hoip*$^{-/-}$ embryos, yet in coabsence of their common receptor, TNFR1, the vascular network is preserved.

Since this phenotype was different from that of *Tnf*$^{-/-}$*Hoip*$^{-/-}$ embryos, we compared the incidence of cell death in both embryos before death. Whereas staining for cleaved caspase-3 showed reoccurrence of cell death at late gestation in *Tnf*$^{-/-}$*Hoip*$^{-/-}$ embryos (Figures 5D and 5E), with cell death being higher at E13.5 than at E15.5 in *Tnf*$^{-/-}$*Hoip*$^{-/-}$ embryos, consistent with the stage at which vascular density starts degenerating again (Figure 4G), in the *Tnfr1*$^{-/-}$*Hoip*$^{-/-}$ embryos, cell death was markedly reduced at both developmental stages and also at E17.5 (i.e., time of death) (Figures 5D and 5E; Figure S5D). Importantly, the significantly reduced, remaining level of cell death (Figures 5D and E) did not disrupt normal vascularization (Figure 5C; Figure S5C). Taken together, these results show that TNFR1 deletion maintains integrity of the yolk sac vascular network of *Hoip*$^{-/-}$ embryos by preventing nonphysiological endothelial cell death induced by TNF and LT-α.

While this result shows that in *Hoip*$^{-/-}$ embryos TNFR1-dependent aberrant cell death is responsible for disruption of yolk sac vascular architecture, other cytokines could be responsible for the remaining cell death observed in *Tnfr1*$^{-/-}$*Hoip*$^{-/-}$ embryos. We therefore tested in vitro whether HOIP-deficient cells were more sensitive to cytokines other than TNF and LT-α and found that this was the case for CD95L, but not for interleukin-1β (IL-1β) and IL-33 (Figure S5E). However, cell death induced by CD95L in the absence of HOIP, as compared to control cells, was not as pronounced as with TNF or LT-α (compare Figures S5E and 5A). Thus, although the remaining cell death observed at late gestation in yolk sacs of *Tnfr1*$^{-/-}$*Hoip*$^{-/-}$ embryos appears to bear no obvious functional consequences on vascularization (Figure 5C), CD95L could be responsible for this cell death.

Despite re-enabling proper yolk sac vascularization, TNFR1 ablation in *Hoip*$^{-/-}$ animals could only further delay death during embryogenesis until E17.5 and not until birth or thereafter. This was surprising given that cIAP1/2-deficient mice are rescued by TNFR1 coablation to birth (Moulin et al., 2012). It therefore appears that LUBAC plays a role in a cIAP1/2-independent pathway that becomes vitally important at around E16.5/17.5 as revealed by the *Tnfr1*$^{-/-}$*Hoip*$^{-/-}$ embryos. To understand the cause of their death, we analyzed them histologically. This revealed severe heart defects, with the atria and large blood vessels of the heart highly dilated and full of blood (Figure 5F). Blood vessels in other organs were also dilated suggesting cardiovascular failure (Figure 5F). Interestingly, this phenotype is not caused by excessive cell death in the heart (Figure 5G), indicating that ablation of TNFR1 rescues cell death both in the

(E) Quantification of cleaved caspase-3 as detected in the images shown in (D); mean ± SEM (n = 4 yolk sacs for *Tnf*$^{-/-}$*Hoip*$^{+/-}$ at E13.5 and E15.5, n = 5 for *Tnf*$^{-/-}$*Hoip*$^{-/-}$ at E13.5, and n = 3 at E15.5; n = 4 for *Tnfr1*$^{-/-}$*Hoip*$^{+/-}$ at E13.5 and E15.5, n = 3 for *Tnfr1*$^{-/-}$*Hoip*$^{-/-}$ at E13.5, and n = 9 at E15.5). Statistics were performed by ANOVA for multiple comparisons ($^{\#}p < 0.001$ *Tnf*$^{-/-}$*Hoip*$^{-/-}$ versus *Tnfr1*$^{-/-}$*Hoip*$^{-/-}$ at E13.5; $^{\Psi}$NS (nonsignificant) *Tnf*$^{-/-}$*Hoip*$^{-/-}$ versus *Tnfr1*$^{-/-}$*Hoip*$^{-/-}$ at E15.5).

(F) Representative images of H&E staining on whole-embryo paraffin sections. A, atrium; V, ventricle; vessels are indicated by an arrow.

(G) Representative images of TUNEL staining on heart sections at E15.5 embryos with quantification. Data are presented as mean ± SEM (n = 3 embryos).

yolk sac and in the heart. Importantly, this phenotype was observed in mutants that were alive (i.e., showing heartbeat), implying the heart defects as a cause, not consequence, of death (Copp, 1995). Intriguingly, a proportion of double-mutant embryos also showed neural tube closure defects of the anterior brain at E10.5 resulting in exencephaly at late gestation (Figure S5F).

Taken together, we show that TNFR1-mediated cell death is causative for disruption of vascularization in HOIP-deficient embryos. However, we also discover that when both HOIP and TNFR1 are absent, morphological defects occur that appear to be independent of cell death but caused by HOIP deficiency.

HOIP-Deficient Cells Fail to Properly Activate NF-κB/MAPKs and Aberrantly Form the Cell-Death-Inducing Complex-II

Having identified aberrant TNFR1-mediated signaling as causative for lethality at midgestation to late gestation due to HOIP absence, we next assessed the molecular impact of HOIP deficiency on TNFR1 signaling. We first tested whether *Hoip*$^{-/-}$ cells still generated linear linkages upon TNF stimulation. To do so, we performed native TNF-RSC analysis as previously described (Gerlach et al., 2011; Haas et al., 2009) from HOIP-deficient versus HOIP-proficient MEFs stimulated with TNF for different times. This revealed the presence of linear linkages in the TNF-RSC in HOIP-proficient, but their complete absence from HOIP-deficient, cells (Figure 6A). Thus, LUBAC is the only ubiquitin E3 generating linear ubiquitin linkages in the TNF-RSC.

We next addressed how the absence of HOIP and, hence, linear ubiquitin from the TNF-RSC affected signaling by TNF and LT-α. We found that NF-κB and MAPK were activated less strongly by both TNF and LT-α in HOIP-deficient MEFs (*Tnf*$^{-/-}$*Hoip*$^{-/-}$) than in control MEFs (*Tnf*$^{-/-}$*Hoip*$^{+/-}$) as observed by delayed phosphorylation and degradation of IκBα and phosphorylation of ERK (Figure 6B). In addition to decreased gene-activatory signaling by the TNF-RSC, and consistent with the increased sensitivity to TNF/LT-α-induced cell death (Figure 5A), we observed increased caspase-3 and caspase-8 cleavage (Figure 6B). As activation of these caspases is known to result from complex-II, we examined whether formation of this complex was aberrantly increased in cells devoid of HOIP in response to TNF. Strikingly, whereas its formation was undetectable in HOIP-proficient cells, complex-II was readily detectable in HOIP-deficient cells with robust recruitment of cleaved caspase-8, RIP1, and RIP3 to FADD (Figure 6C). Thus, absence of HOIP enables the premature and aberrant formation of the cell-death-inducing complex-II of TNFR1 signaling.

Since this complex can mediate apoptotic and necroptotic death (Green et al., 2011; Murphy and Silke, 2014) we next determined the type(s) of cell death induced in HOIP-deficient MEFs. Treatment with the caspase inhibitor Q-Val-Asp(non-O-methylated)-OPh (QVD) or Necrostatin-1, an inhibitor of RIP1's kinase activity, partially blocked TNF-induced death in HOIP-deficient MEFs, which was further reduced by the combination thereof (Figure 6D). Taken together, these results show that deletion of HOIP on the one hand attenuates but does not prevent TNFR1-mediated gene activation and on the other hand markedly increases formation of complex-II, consequently enabling the induction of aberrant cell death upon stimulation by either of its ligands, TNF or LT-α.

HOIP's Catalytic Activity Is Required for Protection from TNF-Induced Cell Death

We finally aimed to determine whether HOIP's catalytic activity is required for protecting cells from TNF-induced death or whether the presence of HOIP, and thus of LUBAC, as a mere scaffold in the TNF-RSC rather than an enzymatically active component is responsible for this effect. To do so, we reconstituted *Tnf*$^{-/-}$*Hoip*$^{-/-}$ MEFs with wild-type (WT) or catalytically inactive (C885S) HOIP. While reconstitution with both forms of HOIP restored expression of HOIL-1 and SHARPIN (Figure 7A), reconstitution with HOIP (C885S) failed to rescue TNF-induced activation of NF-κB and MAPK to normal levels (Figure 7B) and, importantly, also failed to prevent TNF-induced cell death, contrary to reconstitution with WT HOIP (Figure 7C). These results show that HOIP's catalytic activity is required for proper signaling output of the TNF-RSC.

DISCUSSION

Here, we show that constitutive deficiency in the enzymatically active component of LUBAC, HOIP, results in embryonic lethality at midgestation due to disruption of vascularization in the yolk sac and consequent cardiovascular failure. Specific deletion of *Hoip* from endothelial and immune precursor cells with Tie2-promoter-driven Cre resulted in the same phenotype as constitutive deletion of *Hoip*. Both constitutive and endothelial/immune-specific deletion of *Hoip* resulted in a substantial increase in death of endothelial cells in the yolk sac at midgestation, which is causative for disrupted vascularization and, consequently, death. Given that early hematopoiesis takes place in the yolk sac (Inlay et al., 2014), it is difficult to ascertain whether the absence of HOIP from immune cells exerts a direct effect on them or whether the percentage reduction is due to the yolk sac itself degenerating as a consequence of endothelial cell death. However, although an effect of HOIP deficiency on immune cells cannot be formally excluded, given the substantial death of endothelial cells we observe in the yolk sacs of both HOIP-deficient and *Hoip*$^{fl/fl}$*Tie2-Cre*+ embryos, which, importantly, occurs prior to reduction in viability of immune cells, we propose death of endothelial, and not immune, cells as the primary cause of embryonic lethality in *Hoip*$^{-/-}$ and *Hoip*$^{fl/fl}$*Tie2-Cre*+ embryos. The fact that endothelial rather than other cells die in the embryo may be due to differential exposure to TNF and LT-α, which are known to play important roles in secondary lymphoid organ development. Alternatively, endothelial cells may be particularly dependent on HOIP for survival.

Genetic deletion of either TNF or TNFR1 in HOIP-deficient mice prevented cell death in yolk sacs, restored normal vascularization, and, crucially, rescued these embryos from death at E10.5. This implies that endothelial cell death causes disruption of the vascular network and argues against the possibility that HOIP deficiency leads to a defect in developmental pathways, such as angiogenesis. If this were the case, genetic coablation of TNF or TNFR1 would not suppress lethality at midgestation

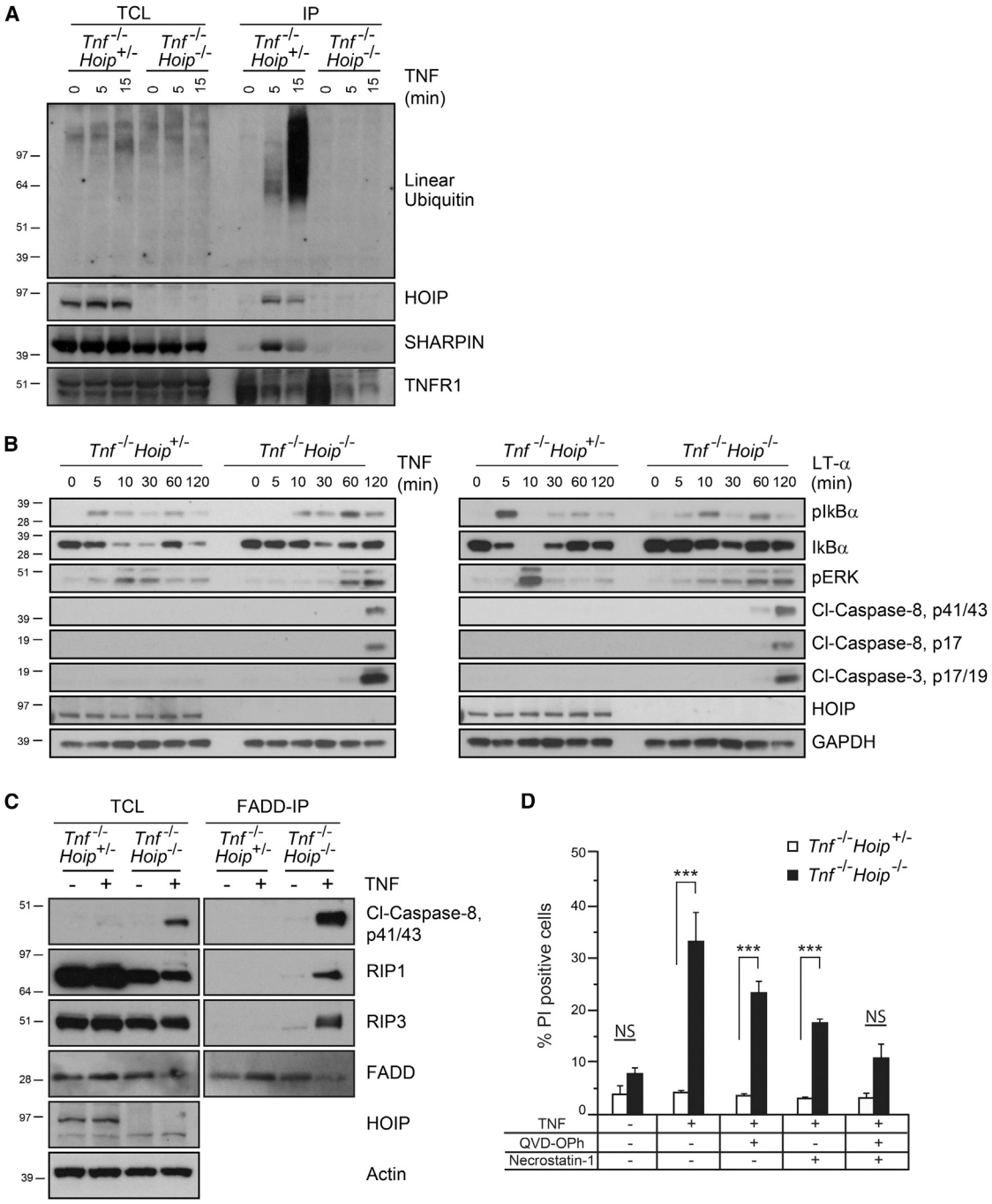

Figure 6. HOIP Is Required for Optimal NF-κB/MAPK Activation and Prevention of Complex-II Formation in Response to TNF

(A) Endogenous TNF-RSC pull-down was performed by TNF immunoprecipitation (IP) in HOIP-proficient and HOIP-deficient cells upon different times of TNF stimulation. Western blot analysis was performed to identify linear ubiquitin chains or the indicated proteins recruited to the complex. TCL, total cellular lysate.

(B) Western blot analysis of the indicated proteins in whole-cell lysates from MEFs following TNF (100 ng/ml) or LT-α (100 ng/ml) stimulation for different time points (min).

(C) FADD immunoprecipitation (IP) was performed in immortalized MEFs treated for 4 hr with 20 μM zVAD-fmk in the presence or absence of TNF (100 ng/ml) for 4 hr. Total cellular lysates (TCL) and IP were analyzed by western blot for the indicated proteins.

(D) Cell death was analyzed by propidium iodide (PI) incorporation in MEFs stimulated with TNF (100 ng/ml) for 24 hr plus the indicated cell death inhibitors. Data are presented as mean ± SEM (n = 3 independent experiments).

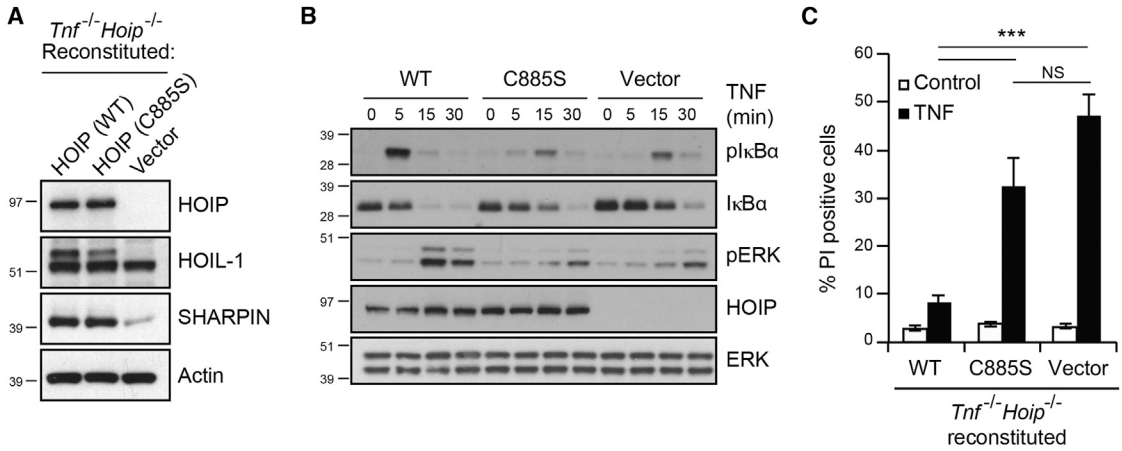

Figure 7. Catalytic Activity of HOIP Is Required for Optimal NF-κB/MAPK Activation and for Protection against Cell Death upon TNF Stimulation

(A) Western blot analysis of the LUBAC components in whole-cell lysates from MEFs reconstituted with wild-type HOIP (WT), catalytically inactive HOIP (C885S), or empty vector.

(B) Western blot analysis of the indicated proteins in whole-cell lysates from *Tnf*$^{-/-}$*Hoip*$^{-/-}$ MEFs reconstituted with the indicated forms of HOIP following TNF (100 ng/ml) stimulation for different time points (min).

(C) PI incorporation in MEFs reconstituted with the indicated forms of HOIP and stimulated with TNF (100 ng/ml). Data are presented as mean ± SEM (n = 3 independent experiments).

in HOIP-deficient embryos. Furthermore, cell death became apparent again in the yolk sac vasculature of *Tnf*$^{-/-}$*Hoip*$^{-/-}$ embryos at E15.5, which coincided with failure of vascularization at this stage. Thus, defective vasculature always occurs together with, and most likely as a consequence of, endothelial cell death. Supporting this notion, cell death in the yolk sac endothelium of *Tnfr1*$^{-/-}$*Hoip*$^{-/-}$ was very low, and the vasculature of these mice was unaffected.

Although LT-α was the first TNF superfamily member to be cloned (Gray et al., 1984) and, like TNF, signals via TNFR1 (Etemadi et al., 2013), TNF is the predominant ligand that drives TNFR1 signaling in vivo, as loss of TNF and TNFR1 phenocopy each other for most functions analyzed so far (Marino et al., 1997; Pasparakis et al., 1996; Rothe et al., 1993). By contrast, deletion of LT-α most closely phenocopies loss of LT-β and LT-βR, since LT-α is required to form heterotrimeric $LT\alpha_1LT\beta_2$ (Browning et al., 1993; Crowe et al., 1994). It is therefore noteworthy that in the pathological scenario of *Hoip* depletion, loss of TNF does not phenocopy loss of TNFR1, indicating a physiological role for the $LT\alpha_3$/TNFR1 signaling.

Histological analysis of *Tnfr1*$^{-/-}$*Hoip*$^{-/-}$ embryos at E15.5 revealed severe morphological defects in the heart, which appear to be independent of cell death. In addition, a proportion of these embryos also exhibited exencephaly. Interestingly, abnormalities in neural crest induction or delamination have previously been shown to account for this particular combination of phenotypes (Barbera et al., 2002), and these abnormalities could therefore also be causative for them in *Tnfr1*$^{-/-}$*Hoip*$^{-/-}$ embryos. It is currently unclear, however, which cell-death-independent pathway is perturbed by absence of HOIP to result in these defects. A mutation in OTULIN, a deubiquitinase that specifically dismantles linear ubiquitin chains, causes embryonic lethality between E12.5 and 14.5. The authors showed that these embryos suffered from deficits in the cranial vasculature and suggested a role for OTULIN in canonical Wnt signaling during angiogenesis (Rivkin et al., 2013). Although we determined the vascular defects in *Hoip*$^{-/-}$ embryos to be due to aberrant endothelial cell death rather than defective angiogenesis, *Tnfr1*$^{-/-}$*Hoip*$^{-/-}$ embryos had dramatic defects in the heart, most likely caused by aberrant neural crest induction. It is tempting to speculate that proper Wnt signaling, known to be required for various developmental processes during embryogenesis (Copp, 1995; van Amerongen and Berns, 2006), could be perturbed in HOIP's absence and thereby responsible for the phenotype of *Tnfr1*$^{-/-}$*Hoip*$^{-/-}$ embryos.

Reconstitution experiments performed in this study show that not only the physical presence of HOIP and LUBAC but also its catalytic activity in the TNF-RSC is required to prevent TNF-induced cell death. This result is in accordance with the recent mentioning of HOIP's catalytic activity as essential for embryogenesis (Emmerich et al., 2013). Together, this shows that LUBAC and its linear-ubiquitin-forming activity are required to inhibit TNF-induced death for proper embryogenesis.

LUBAC forms part of the TNF-RSC and contributes to full NF-κB activation. However, the findings we report here, in conjunction with the reported phenotypes of mice devoid of individual components of the TNF-triggered gene-activatory and cell death pathways, respectively, allow us to deduce that it is indeed the lack of proper control of cell death, importantly independently of the gene-activatory role of LUBAC, which is responsible for lethality of HOIP deficiency. The rationale for this conclusion is laid out in the next paragraph.

Indeed, we observed attenuated gene-activatory signaling in TNF- and LT-α-stimulated *Tnf*$^{-/-}$*Hoip*$^{-/-}$ MEFs, confirming a role for LUBAC in maintaining optimal NF-κB activation by the

TNF-RSC. Yet, while NF-κB activation was only reduced, there was a robust formation of complex-II in HOIP-deficient cells upon TNF stimulation, which did not occur in HOIP-proficient cells. It therefore appears that aberrant complex-II formation is responsible for nonphysiological TNFR1-mediated death of endothelial cells in the yolk sac and, consequently, embryonic lethality of HOIP deficiency at midgestation. However, this alone would be insufficient to conclude that attenuated NF-κB-mediated gene activation would not play a role in rendering cells more TNF sensitive in the absence of HOIP. Yet, if attenuated NF-κB activation were responsible, then mice with a complete lack in NF-κB activation should die at least as early as HOIP-deficient mice. This is, however, not the case. Instead, IKKα-deficient mice die perinatally (Takeda et al., 1999), and IKKβ and NEMO/IKKγ deficiency results in embryonic lethality at late gestation (E12.5/14.5), yet from liver injury (Rudolph et al., 2000; Schmidt-Supprian et al., 2000; Tanaka et al., 1999), hence a phenotype very different from the one we observed in *Hoip*$^{-/-}$ embryos. On the contrary, deficiency in components of the cell death complex, such as caspase-8, FADD, and FLIP, results in embryonic lethality at midgestation, precisely at E10.5 (Varfolomeev et al., 1998; Yeh et al., 1998, 2000; Zhang et al., 1998), which, intriguingly, is also when caspase-8 was specifically deleted in endothelial cells (Kang et al., 2004). Importantly, these deaths at midgestation were recently revealed to be due to aberrant necroptotic and/or apoptotic cell death, depending on which component was deleted (Dillon et al., 2012; Kaiser et al., 2011; Oberst et al., 2011; Zhang et al., 2011).

Together, our findings indicate that LUBAC-dependent cell death regulation is crucial for proper vascularization during midstages of embryogenesis and that the phenotype of HOIP-deficient embryos mimics the ones observed in the absence of cell-death-associated components. It will be interesting to assess the effect of interference with apoptosis and/or necroptosis by their concomitant genetic coinactivation (Dillon et al., 2012; Kaiser et al., 2011). However, this analysis cannot realistically be achieved by conventional breeding strategies, since the genes encoding HOIP and RIP3 are located within 200 kbp of each other on chromosome 14 in mice.

In summary, we propose that due to lack of linear ubiquitination, the balance between TNF-induced gene activation and cell death is disturbed in HOIP-deficient embryos in favor of cell death and that the nonphysiological cell death resulting from this disbalance is responsible for the lethality caused by HOIP deficiency at midgestation.

EXPERIMENTAL PROCEDURES

Mice

The HOIP-deficient mouse strain used for this study was created from embryonic stem cell clone EPD0161_5_A05 obtained from KOMP Repository (http://www.komp.org) and generated by the Wellcome Trust Sanger Institute. Methods used on the targeted alleles have been previously described (Skarnes et al., 2011). The targeting cassette was composed of a lacZ reporter gene plus a neomycin cassette flanked by Frt sites and exons 6 (ENSMUSE00000316844) to 11 (ENSMUSE00000316820) of the *hoip* gene flanked by loxP sites. The mice were generated via C57BL/6N ES cell microinjection into BALB/c blastocysts to generate chimeric mice, which were bred for germline transmission through the ES Cell to Mouse service of the Australian Phenomics Network. The chimeric progeny were bred to generate HOIP-floxed animals. The neomycin cassette was removed by crossing these mice with mice expressing the frt-deleter FlpE recombinase (C57BL/6J) (Farley et al., 2000) to remove the reporter gene. Subsequently, the progeny was crossed with transgenic mice expressing the loxP-deleter Cre recombinase purchased from JAX (6054, B6.C-Tg[CMV-Cre]1 Cgn/J) to generate full-knockout animals. Alternatively, transgenic mice expressing the Cre recombinase under the control of the Tie2 promoter (*Tie2*-Cre) (B6.Cg-Tg[Tek-cre]1Ywa/J) (Gustafsson et al., 2001) were crossed with HOIP-floxed animals to delete HOIP specifically in endothelial cells. *Tnf*$^{-/-}$ mice were a gift from William Kaiser (B6;129S6), and *Tnfr1*$^{-/-}$ mice were purchased from JAX (2818, B6.129-Tnfrsf1atm1Mak/J). All mice were crossed for at least five generations before the embryological studies. All mice were typed by PCR analysis. Colonies were fed ad libitum and kept under an appropriate UK project license.

Timed Matings, Histological Analysis, and In Situ Hybridization

A single male was paired with one or two females, which were plug checked daily. The embryonic days were counted starting E0.5 on the day the vaginal plug was detected. The embryos were taken from the mothers at different developmental stages, fixed in 4% paraformaldehyde for 24 hr, refrigerated, and stored in methanol for further analysis. For histological purposes, embryos were paraffin embedded, and serial sections of 4 μm were performed. Sections were stained with hematoxylin and eosin (H&E). Eight sagittal serial sections of two different planes of the embryo were analyzed by a pathologist. In situ hybridization of whole-mount embryos was performed by standard procedures (Behringer, 2003). The probe was generated by cloning a 1.3 kb region of *Hoip* cDNA in pcDNA3 vector. Sense and antisense probes were generated by in vitro transcription using digoxigenin-labeled dinucleotide triphosphates and SP6 and T7 promoters, respectively.

Statistical Analysis

Statistical significance was determined using unpaired Student's t test. A p value < 0.05 was considered significant and indicated with $^{*}p < 0.05$, $^{**}p < 0.01$, and $^{***}p < 0.001$. Alternatively, whenever stated, ANOVA for multiple comparisons was used.

SUPPLEMENTAL INFORMATION

Supplemental Information includes Supplemental Experimental Procedures and five figures and can be found with this article online at http://dx.doi.org/10.1016/j.celrep.2014.08.066.

AUTHOR CONTRIBUTIONS

H.W., T.A.R., N.P., and E.R. designed the research. N.P. and H.W. wrote the manuscript. N.P. performed the majority of experiments; E.R., L.T., P.D., M.D., A.M., B.P., and Y.S. contributed experimentally; A.S. and H.D. contributed experimentally and with mouse maintenance and genotyping; J.P.M.-B. performed the pathology; and J.S. contributed to the generation of HOIP-floxed animals and discussion of results and manuscript.

ACKNOWLEDGMENTS

We thank Vishva Dixit and Domagoj Vucic from Genentech (South San Francisco, CA) for the linear-ubiquitin-specific antibody; Alessandro Annibaldi from The Breakthrough Toby Robins Breast Cancer Research Centre, Institute of Cancer Research (London, UK) for helpful discussions; Aida Di Gregorio and Juan Miguel Sanchez Nieto at NHLI, Imperial College (London, UK) for technical assistance; Lorraine Lawrence at NHLI, Imperial College (London, UK) for histology services; and Arnold Pizzey at the UCL Cancer Institute (London, UK) for technical support with cell sorting experiments. This work was funded by a Wellcome Trust Senior Investigator Award (096831/Z/11/Z), a NHMRC grant awarded to J.S. and H.W. (602516) an ERC Advanced grant (294880) awarded to H.W., and a postdoctoral fellowship awarded to N.P. by the Swiss National Science Foundation (P2LAP3_148447).

Received: April 15, 2014
Revised: July 31, 2014
Accepted: August 26, 2014
Published: October 2, 2014

REFERENCES

Aggarwal, B.B., Eessalu, T.E., and Hass, P.E. (1985). Characterization of receptors for human tumour necrosis factor and their regulation by gamma-interferon. Nature *318*, 665–667.

Barbera, J.P., Rodriguez, T.A., Greene, N.D., Weninger, W.J., Simeone, A., Copp, A.J., Beddington, R.S., and Dunwoodie, S. (2002). Folic acid prevents exencephaly in Cited2 deficient mice. Hum. Mol. Genet. *11*, 283–293.

Behringer, R. (2003). Manipulating the Mouse Embryo: A Laboratory Manual, Third Edition (Cold Spring Harbor: Cold Spring Harbor Laboratory Press).

Browning, J.L., Ngam-ek, A., Lawton, P., DeMarinis, J., Tizard, R., Chow, E.P., Hession, C., O'Brine-Greco, B., Foley, S.F., and Ware, C.F. (1993). Lymphotoxin beta, a novel member of the TNF family that forms a heteromeric complex with lymphotoxin on the cell surface. Cell *72*, 847–856.

Copp, A.J. (1995). Death before birth: clues from gene knockouts and mutations. Trends Genet. *11*, 87–93.

Crowe, P.D., VanArsdale, T.L., Walter, B.N., Ware, C.F., Hession, C., Ehrenfels, B., Browning, J.L., Din, W.S., Goodwin, R.G., and Smith, C.A. (1994). A lymphotoxin-beta-specific receptor. Science *264*, 707–710.

Damgaard, R.B., Nachbur, U., Yabal, M., Wong, W.W., Fiil, B.K., Kastirr, M., Rieser, E., Rickard, J.A., Bankovacki, A., Peschel, C., et al. (2012). The ubiquitin ligase XIAP recruits LUBAC for NOD2 signaling in inflammation and innate immunity. Mol. Cell *46*, 746–758.

Dillon, C.P., Oberst, A., Weinlich, R., Janke, L.J., Kang, T.B., Ben-Moshe, T., Mak, T.W., Wallach, D., and Green, D.R. (2012). Survival function of the FADD-CASPASE-8-cFLIP(L) complex. Cell Reports *1*, 401–407.

Emmerich, C.H., Ordureau, A., Strickson, S., Arthur, J.S., Pedrioli, P.G., Komander, D., and Cohen, P. (2013). Activation of the canonical IKK complex by K63/M1-linked hybrid ubiquitin chains. Proc. Natl. Acad. Sci. USA *110*, 15247–15252.

Etemadi, N., Holien, J.K., Chau, D., Dewson, G., Murphy, J.M., Alexander, W.S., Parker, M.W., Silke, J., and Nachbur, U. (2013). Lymphotoxin α induces apoptosis, necroptosis and inflammatory signals with the same potency as tumour necrosis factor. FEBS J. *280*, 5283–5297.

Farley, F.W., Soriano, P., Steffen, L.S., and Dymecki, S.M. (2000). Widespread recombinase expression using FLPeR (flipper) mice. Genesis *28*, 106–110.

Gerlach, B., Cordier, S.M., Schmukle, A.C., Emmerich, C.H., Rieser, E., Haas, T.L., Webb, A.I., Rickard, J.A., Anderton, H., Wong, W.W., et al. (2011). Linear ubiquitination prevents inflammation and regulates immune signalling. Nature *471*, 591–596.

Gray, P.W., Aggarwal, B.B., Benton, C.V., Bringman, T.S., Henzel, W.J., Jarrett, J.A., Leung, D.W., Moffat, B., Ng, P., Svedersky, L.P., et al. (1984). Cloning and expression of cDNA for human lymphotoxin, a lymphokine with tumour necrosis activity. Nature *312*, 721–724.

Green, D.R., Oberst, A., Dillon, C.P., Weinlich, R., and Salvesen, G.S. (2011). RIPK-dependent necrosis and its regulation by caspases: a mystery in five acts. Mol. Cell *44*, 9–16.

Gustafsson, E., Brakebusch, C., Hietanen, K., and Fässler, R. (2001). Tie-1-directed expression of Cre recombinase in endothelial cells of embryoid bodies and transgenic mice. J. Cell Sci. *114*, 671–676.

Haar, J.L., and Ackerman, G.A. (1971). A phase and electron microscopic study of vasculogenesis and erythropoiesis in the yolk sac of the mouse. Anat. Rec. *170*, 199–223.

Haas, T.L., Emmerich, C.H., Gerlach, B., Schmukle, A.C., Cordier, S.M., Rieser, E., Feltham, R., Vince, J., Warnken, U., Wenger, T., et al. (2009). Recruitment of the linear ubiquitin chain assembly complex stabilizes the TNF-R1 signaling complex and is required for TNF-mediated gene induction. Mol. Cell *36*, 831–844.

Hamaguchi, I., Morisada, T., Azuma, M., Murakami, K., Kuramitsu, M., Mizukami, T., Ohbo, K., Yamaguchi, K., Oike, Y., Dumont, D.J., and Suda, T. (2006). Loss of Tie2 receptor compromises embryonic stem cell-derived endothelial but not hematopoietic cell survival. Blood *107*, 1207–1213.

Ikeda, F., Deribe, Y.L., Skånland, S.S., Stieglitz, B., Grabbe, C., Franz-Wachtel, M., van Wijk, S.J., Goswami, P., Nagy, V., Terzic, J., et al. (2011). SHARPIN forms a linear ubiquitin ligase complex regulating NF-κB activity and apoptosis. Nature *471*, 637–641.

Inlay, M.A., Serwold, T., Mosley, A., Fathman, J.W., Dimov, I.K., Seita, J., and Weissman, I.L. (2014). Identification of multipotent progenitors that emerge prior to hematopoietic stem cells in embryonic development. Stem Cell Reports *2*, 457–472.

Iwai, K., Fujita, H., and Sasaki, Y. (2014). Linear ubiquitin chains. NF-κB signalling, cell death and beyond. Nat. Rev. Mol. Cell Biol. *15*, 503–508.

Kaiser, W.J., Upton, J.W., Long, A.B., Livingston-Rosanoff, D., Daley-Bauer, L.P., Hakem, R., Caspary, T., and Mocarski, E.S. (2011). RIP3 mediates the embryonic lethality of caspase-8-deficient mice. Nature *471*, 368–372.

Kang, T.B., Ben-Moshe, T., Varfolomeev, E.E., Pewzner-Jung, Y., Yogev, N., Jurewicz, A., Waisman, A., Brenner, O., Haffner, R., Gustafsson, E., et al. (2004). Caspase-8 serves both apoptotic and nonapoptotic roles. J. Immunol. *173*, 2976–2984.

Komander, D. (2009). The emerging complexity of protein ubiquitination. Biochem. Soc. Trans. *37*, 937–953.

Marino, M.W., Dunn, A., Grail, D., Inglese, M., Noguchi, Y., Richards, E., Jungbluth, A., Wada, H., Moore, M., Williamson, B., et al. (1997). Characterization of tumor necrosis factor-deficient mice. Proc. Natl. Acad. Sci. USA *94*, 8093–8098.

Micheau, O., and Tschopp, J. (2003). Induction of TNF receptor I-mediated apoptosis via two sequential signaling complexes. Cell *114*, 181–190.

Moulin, M., Anderton, H., Voss, A.K., Thomas, T., Wong, W.W., Bankovacki, A., Feltham, R., Chau, D., Cook, W.D., Silke, J., and Vaux, D.L. (2012). IAPs limit activation of RIP kinases by TNF receptor 1 during development. EMBO J. *31*, 1679–1691.

Murphy, J.M., and Silke, J. (2014). Ars Moriendi; the art of dying well - new insights into the molecular pathways of necroptotic cell death. EMBO Rep. *15*, 155–164.

Oberst, A., Dillon, C.P., Weinlich, R., McCormick, L.L., Fitzgerald, P., Pop, C., Hakem, R., Salvesen, G.S., and Green, D.R. (2011). Catalytic activity of the caspase-8-FLIP(L) complex inhibits RIPK3-dependent necrosis. Nature *471*, 363–367.

Pasparakis, M., Alexopoulou, L., Episkopou, V., and Kollias, G. (1996). Immune and inflammatory responses in TNF alpha-deficient mice: a critical requirement for TNF alpha in the formation of primary B cell follicles, follicular dendritic cell networks and germinal centers, and in the maturation of the humoral immune response. J. Exp. Med. *184*, 1397–1411.

Rieser, E., Cordier, S.M., and Walczak, H. (2013). Linear ubiquitination: a newly discovered regulator of cell signalling. Trends Biochem. Sci. *38*, 94–102.

Rivkin, E., Almeida, S.M., Ceccarelli, D.F., Juang, Y.C., MacLean, T.A., Srikumar, T., Huang, H., Dunham, W.H., Fukumura, R., Xie, G., et al. (2013). The linear ubiquitin-specific deubiquitinase gumby regulates angiogenesis. Nature *498*, 318–324.

Rothe, J., Lesslauer, W., Lötscher, H., Lang, Y., Koebel, P., Köntgen, F., Althage, A., Zinkernagel, R., Steinmetz, M., and Bluethmann, H. (1993). Mice lacking the tumour necrosis factor receptor 1 are resistant to TNF-mediated toxicity but highly susceptible to infection by Listeria monocytogenes. Nature *364*, 798–802.

Rudolph, D., Yeh, W.C., Wakeham, A., Rudolph, B., Nallainathan, D., Potter, J., Elia, A.J., and Mak, T.W. (2000). Severe liver degeneration and lack of NF-kappaB activation in NEMO/IKKgamma-deficient mice. Genes Dev. *14*, 854–862.

Sasaki, Y., Sano, S., Nakahara, M., Murata, S., Kometani, K., Aiba, Y., Sakamoto, S., Watanabe, Y., Tanaka, K., Kurosaki, T., and Iwai, K. (2013). Defective immune responses in mice lacking LUBAC-mediated linear ubiquitination in B cells. EMBO J. *32*, 2463–2476.

Schmidt-Supprian, M., Bloch, W., Courtois, G., Addicks, K., Israël, A., Rajewsky, K., and Pasparakis, M. (2000). NEMO/IKK gamma-deficient mice model incontinentia pigmenti. Mol. Cell *5*, 981–992.

Schmukle, A.C., and Walczak, H. (2012). No one can whistle a symphony alone - how different ubiquitin linkages cooperate to orchestrate NF-κB activity. J. Cell Sci. *125*, 549–559.

Seymour, R.E., Hasham, M.G., Cox, G.A., Shultz, L.D., Hogenesch, H., Roopenian, D.C., and Sundberg, J.P. (2007). Spontaneous mutations in the mouse Sharpin gene result in multiorgan inflammation, immune system dysregulation and dermatitis. Genes Immun. *8*, 416–421.

Skarnes, W.C., Rosen, B., West, A.P., Koutsourakis, M., Bushell, W., Iyer, V., Mujica, A.O., Thomas, M., Harrow, J., Cox, T., et al. (2011). A conditional knockout resource for the genome-wide study of mouse gene function. Nature *474*, 337–342.

Takeda, K., Takeuchi, O., Tsujimura, T., Itami, S., Adachi, O., Kawai, T., Sanjo, H., Yoshikawa, K., Terada, N., and Akira, S. (1999). Limb and skin abnormalities in mice lacking IKKalpha. Science *284*, 313–316.

Tanaka, M., Fuentes, M.E., Yamaguchi, K., Durnin, M.H., Dalrymple, S.A., Hardy, K.L., and Goeddel, D.V. (1999). Embryonic lethality, liver degeneration, and impaired NF-kappa B activation in IKK-beta-deficient mice. Immunity *10*, 421–429.

Tenev, T., Bianchi, K., Darding, M., Broemer, M., Langlais, C., Wallberg, F., Zachariou, A., Lopez, J., MacFarlane, M., Cain, K., and Meier, P. (2011). The Ripoptosome, a signaling platform that assembles in response to genotoxic stress and loss of IAPs. Mol. Cell *43*, 432–448.

Tokunaga, F., Sakata, S., Saeki, Y., Satomi, Y., Kirisako, T., Kamei, K., Nakagawa, T., Kato, M., Murata, S., Yamaoka, S., et al. (2009). Involvement of linear polyubiquitylation of NEMO in NF-kappaB activation. Nat. Cell Biol. *11*, 123–132.

Tokunaga, F., Nakagawa, T., Nakahara, M., Saeki, Y., Taniguchi, M., Sakata, S., Tanaka, K., Nakano, H., and Iwai, K. (2011). SHARPIN is a component of the NF-κB-activating linear ubiquitin chain assembly complex. Nature *471*, 633–636.

van Amerongen, R., and Berns, A. (2006). Knockout mouse models to study Wnt signal transduction. Trends Genet. *22*, 678–689.

Varfolomeev, E.E., Schuchmann, M., Luria, V., Chiannilkulchai, N., Beckmann, J.S., Mett, I.L., Rebrikov, D., Brodianski, V.M., Kemper, O.C., Kollet, O., et al. (1998). Targeted disruption of the mouse Caspase 8 gene ablates cell death induction by the TNF receptors, Fas/Apo1, and DR3 and is lethal prenatally. Immunity *9*, 267–276.

Walczak, H., Iwai, K., and Dikic, I. (2012). Generation and physiological roles of linear ubiquitin chains. BMC Biol. *10*, 23.

Yeh, W.C., de la Pompa, J.L., McCurrach, M.E., Shu, H.B., Elia, A.J., Shahinian, A., Ng, M., Wakeham, A., Khoo, W., Mitchell, K., et al. (1998). FADD: essential for embryo development and signaling from some, but not all, inducers of apoptosis. Science *279*, 1954–1958.

Yeh, W.C., Itie, A., Elia, A.J., Ng, M., Shu, H.B., Wakeham, A., Mirtsos, C., Suzuki, N., Bonnard, M., Goeddel, D.V., and Mak, T.W. (2000). Requirement for Casper (c-FLIP) in regulation of death receptor-induced apoptosis and embryonic development. Immunity *12*, 633–642.

Zak, D.E., Schmitz, F., Gold, E.S., Diercks, A.H., Peschon, J.J., Valvo, J.S., Niemistö, A., Podolsky, I., Fallen, S.G., Suen, R., et al. (2011). Systems analysis identifies an essential role for SHANK-associated RH domain-interacting protein (SHARPIN) in macrophage Toll-like receptor 2 (TLR2) responses. Proc. Natl. Acad. Sci. USA *108*, 11536–11541.

Zhang, J., Cado, D., Chen, A., Kabra, N.H., and Winoto, A. (1998). Fas-mediated apoptosis and activation-induced T-cell proliferation are defective in mice lacking FADD/Mort1. Nature *392*, 296–300.

Zhang, H., Zhou, X., McQuade, T., Li, J., Chan, F.K., and Zhang, J. (2011). Functional complementation between FADD and RIP1 in embryos and lymphocytes. Nature *471*, 373–376.

Zinngrebe, J., Montinaro, A., Peltzer, N., and Walczak, H. (2014). Ubiquitin in the immune system. EMBO Rep. *15*, 28–45.